Nečada, Marek; Martikainen, Jani Petri; Törmä, Päivi

Quantum emitter dipole-dipole interactions in nanoplasmonic systems

Published in:
International Journal of Modern Physics B

DOI:
10.1142/S0217979217400069

Published: 30/09/2017

Document Version
Publisher's PDF, also known as Version of record

Please cite the original version:
Nečada, M., Martikainen, J. P., & Törmä, P. (2017). Quantum emitter dipole-dipole interactions in nanoplasmonic systems. *International Journal of Modern Physics B*, *31*(24), 1-21. Article 1740006. https://doi.org/10.1142/S0217979217400069

International Journal of Modern Physics B
Vol. 31, No. 24 (2017) 1740006 (21 pages)

DOI: 10.1142/S0217979217400069

Quantum emitter dipole–dipole interactions in nanoplasmonic systems

Marek Nečada,* Jani-Petri Martikainen and Päivi Törmä†
COMP Centre of Excellence, Department of Applied Physics,
Aalto University, P.O. Box 15100,
FI-00076 Aalto, Finland
**marek.necada@aalto.fi; marek@necada.org*
†*paivi.torma@aalto.fi*

Received 6 April 2017
Revised 19 June 2017
Accepted 20 June 2017
Published 1 August 2017

We introduce a generalized Dicke-like model to describe two-level systems coupled with a single bosonic mode. In addition, the two-level systems mutually interact via direct dipole–dipole interaction. We apply the model to an ensemble of dye molecules coupled to a plasmonic excitation in a metallic nanoparticle and study how the dipole–dipole interaction and configurational randomness introduced to the system affect the energy spectra. Comparing the system eigenenergies obtained by our model with the light spectra from a multiple-scattering simulation, we suggest a way to identify dark modes in our model. Finally, we perform a parameter sweep in order to determine the scaling properties of the system and to classify the regions of the parameter space where the dipole–dipole interactions can have significant effects.

Keywords: Quantum emitters; dipole–dipole interactions; nanoplasmics; nano-optics; Dicke model.

PACS numbers: 42.50.Ct, 42.50.Nn, 33.50.-j, 73.20.Mf

1. Introduction

Surface plasmon polaritons (SPPs) are hybrid modes of electron plasma oscillations inside metals and the electromagnetic field inside and outside of the metallic structure. At resonant frequencies, which are determined by the plasma frequency of the bulk metal and the nanostructure geometry, the intensity of the SPP modes in the near field is significantly magnified. This field enhancement can lead to strong coupling between the SPP and quantum emitters (QEs) located in the vicinity of

*Corresponding author.

the metal surface, creating a hybrid mode consisting of the SPP and the QE excitations. The strong coupling manifests itself as an avoided crossing between the original SPP and QE energy levels, as has been experimentally realized in various nanoplasmonic structures; see the review[22] and works[1,2,18,24] that appeared afterwards, and references therein; for theory, see Refs. 5 and 9 and the review.[22]

Here we address *the question whether the dipole–dipole interactions between the QEs can play a role in such systems*. To our knowledge, there has not been any experimental evidence of this, but theoretical works exist that allow for such a possibility. A study by Salomon *et al.*[16] using the finite-difference time-domain (FDTD) solution of Maxwell–Liouville equations for a silver slit array covered by a thin layer of molecules presented a possibility for an additional mode in the transmission spectra between the avoided strong coupling modes, provided that either molecules concentration or their transition dipole moment is large enough. A multiple-scattering method based on macroscopic quantum electrodynamics was used by Delga *et al.*[4,5] to show similar results for a system of single spherical nanoparticle with adjacent fluorescent molecules. Here we answer this question by a different approach, namely a modified Dicke model.

Interactions between electromagnetic fields and a collection of QEs such as atoms or fluorescent molecules are of interest in many areas of physics. The simplest quantum model of such a system is the original Dicke model,[6] where identical two-level systems (TLS) are coupled to a single-harmonic oscillator-like field mode, all with the same coupling strength, and without direct mutual coupling. Dicke model can be solved exactly using the algebraic Bethe ansatz.[8] There also exists an exact solution for an extended Dicke model which includes direct coupling term between the QEs,[13] but the coupling strengths between each pair of QEs must all be equal, as well as the QE–field mode couplings, which is unrealistic for real systems with many QEs. In this paper, we study a model in which *all the coupling strengths of both types of couplings can vary*, which is expected to happen in real systems where the QEs can have various positions and orientations. The price of relaxing these constraints is the impossibility to diagonalize the Hamiltonian with the Bethe ansatz, so we use the numerical exact diagonalization instead.

The original Dicke model describes well a system of atoms in a high-Q optical nanocavity, as long as the atoms are separated well enough so that their mutual dipole–dipole interactions are negligible and the cavity supports single radiation mode near the resonant frequency of the atoms, and the other modes are well separated. However, our motivation stems from the study of nanoplasmonic systems where QEs interact with SPP modes supported by a metallic nanostructure. In the nanoplasmonic systems, the coupling strengths between the QEs and the SPP vary considerably depending on the configuration of the QEs. In particular, we are interested whether the dipole–dipole couplings between the QEs can have significant effect on the system.

Approaches different from ours have been developed to model the behavior of the nanoplasmonic systems in question. Among the notable ones are the methods

based on FDTD solution of Maxwell–Liouville equations[19] and quantum multiple-scattering methods based on macroscopic quantum electrodynamics,[23] which have their advantages and disadvantages. Most notably, they account for the Ohmic losses inside the metal and the consequent line broadening which are significant in plasmonic systems. On the other hand, our modified Dicke model is much less computationally expensive and gives intuitive understanding of the problem. Another approach aims to solve the system dynamics using Lindblad equations.[21] We compare our model with the multiple-scattering approach (which includes all multipoles) in Sec. 4 of this paper for a system of quantum emitters in the vicinity of a single nanoparticle. We make the comparison both in the dipole approximation and also by including higher-order multipole modes of the nanoparticle.

This paper is organized as follows. In Sec. 2, we generalize the extended Dicke model[13] by relaxing its equal-coupling symmetries. In Sec. 3, we briefly sketch the principles of the multiple-scattering method, which is used as a benchmark for our model in Sec. 4, where for some example configurations, we compare the resulting energy levels with the far-field light spectra obtained by multiple-scattering method as shown by Delga *et al.*,[4] observing a clear correspondence between them. Although our model does not by itself include any information about the visibility of its eigenenergies, we find an observable which identifies the dark modes. Finally, in Sec. 5 we use our relaxed Dicke model to perform a parameter sweep in the single excitation subspace with the goal of identifying the effects of varying dipole–dipole interactions in the model and their relevance for the parameters typical in the experiments with quantum emitters near plasmonic nanostructures. In Sec. 6, we discuss what conditions would the system have to satisfy in order to make the effects of the dipole–dipole interactions observable.

2. The Relaxed Dicke Model

We consider an ensemble of K identical quantum emitters — modeled as two-level systems — interacting with a single-field mode. Our model Hamiltonian of the system (utilizing the rotating wave approximation) is

$$H = \hbar\omega\hat{b}^\dagger\hat{b} + \sum_i \hbar\epsilon\left(\hat{S}_i^z + \frac{1}{2}\right) + \sum_i V_i(\hat{b}^\dagger\hat{S}_i^- + \hat{S}_i^+\hat{b}) + \sum_{i<j} g_{ij}(\hat{S}_i^+\hat{S}_j^- + \hat{S}_j^+S_i^-), \quad (1)$$

where ω is the frequency of the field mode, ϵ is the resonant frequency of the atoms, V_i is the coupling coefficient between the ith atom and the field mode and g_{ij} are the coefficients of the direct interaction between the ith and the jth atoms. Here $\hat{S}_i^+$, $\hat{S}_i^-$ and $\hat{S}_i^z$ are spin-1/2 operators given by

$$\hat{S}_i^+ = |g_i\rangle\langle e_i|, \quad \hat{S}_i^- = |e_i\rangle\langle g_i|, \quad \hat{S}_i^z = \frac{1}{2}(|e_i\rangle\langle e_i| - |g_i\rangle\langle g_i|),$$

where $|g_i\rangle$ and $|e_i\rangle$ are the ground and excited states of the ith atom; $\hat{b}^\dagger, \hat{b}$ are the creation and annihilation operators of the field mode, satisfying the usual bosonic commutation relation $[\hat{b}, \hat{b}^\dagger] = 1$.

The extended Dicke model solved by Pan *et al.*[13] has the same form as (1) but it assumes that the dipole–dipole and dipole–field couplings are constant, $g_{ij} = g$ and $V_i = V$ (in addition, $g_{ij} = 0$ in the original Dicke model). In contrast, in our model the coupling constants in the atom–atom and atom–field interactions may vary, relaxing the symmetries which enable the Dicke model to be exactly solvable by the Bethe ansatz. On the other hand, our model provides much more realistic description of the physical systems in which we are interested. A typical realization of our model would consist of quantum emitters (e.g., dye molecules embedded into polymer matrix) in a cavity or in the vicinity of a waveguide or a nanoparticle supporting a single dominant EM field mode — meaning that for at least a certain time scale, the remainder of the electromagnetic spectrum as well as the nonradiative losses can be neglected. The quantum emitters are deposited randomly both in positions and dipole orientations, which leads to some random distribution of the dipole–dipole coupling strengths g_{ij}.

We assume that the system does not reach ultrastrong coupling regime, which would invalidate the rotating wave approximation.[17] Thanks to the approximation, the total excitation number operator $\hat{N} = \hat{b}^\dagger\hat{b} + \sum_i(\hat{S}_i^z + \frac{1}{2})$ commutes with the Hamiltonian; the total excitation number thus remains conserved and the Hamiltonian can be diagonalized for each excitation number subspace separately, which allows us to reduce the computational requirements of diagonalization. In the following, we deal mainly with the single excitation subspace ($N = 1$) which is generated by the states $\hat{b}^\dagger|g\rangle, \hat{S}_i^+|g\rangle$ where $|g\rangle = (|0\rangle \otimes \prod_j |g_j\rangle)$ is the ground state of the whole system and $|0\rangle$ is the vacuum of the bosonic part.

Let us describe how the Hamiltonian (1) and its parameters can be derived for a subwavelength-sized system of a plasmonic resonator and adjacent emitters. The resonator mode alone is obtained by solving macroscopic Maxwell's equations with the respective constitutive relations. If the system is not limited to a finite volume, this usually yields a continuum of mutually orthogonal solutions with infinite mode volumes (and thus energies). This can be worked around[7] by using, for example, a quasistatic approximation (i.e., assuming infinite speed of light) where the problem is reduced to Gauss law,

$$\nabla \cdot (\varepsilon(\omega, \boldsymbol{r})\boldsymbol{E}(\boldsymbol{r})) = 0, \tag{2}$$

with appropriate boundary conditions. The electric field of the quasistatic modes is a Coulombic field from bound charges in the resonator, and therefore fully longitudinal. The quasistatic approximation eliminates the losses due to the radiation and leads to discrete spectrum in ω. In order to make the spectrum real, we further neglect the imaginary part of $\varepsilon(\omega, \boldsymbol{r})$ for real ω, thus eliminating the internal losses of the material and making the plasmonic resonator a closed system. At this point, we get from (2) a discrete set of quasistatic modes with the dynamics of a harmonic

oscillator, which — after the usual quantization procedure and dropping the zero point energy — yields the resonator part of the Hamiltonian,

$$H_{\rm res} = \hbar \sum_\lambda \omega_\lambda \hat{b}_\lambda^\dagger \hat{b}_\lambda,$$

and the electric field operator has the form

$$\hat{\boldsymbol{E}}(\boldsymbol{r}) = \sum_\lambda \sqrt{\frac{\hbar\omega_\lambda}{2U_\lambda \varepsilon_0}} (\boldsymbol{E}_\lambda(\boldsymbol{r})\hat{b}_\lambda + \boldsymbol{E}_\lambda^*(\boldsymbol{r})\,\hat{b}_\lambda^\dagger), \tag{3}$$

where $\omega_\lambda, \boldsymbol{E}_\lambda(\boldsymbol{r})$ are the solutions of the classical equation (2). The operator is normalized by the quasistatic mode energies $U_\lambda = \varepsilon_0 \int d^3\boldsymbol{r}\, |\boldsymbol{E}_\lambda(\boldsymbol{r})|^2/2$. In Appendix A, we show how to derive the expression for $\hat{\boldsymbol{E}}(\boldsymbol{r})$ for the quasistatic modes of a spherical nanoparticle.

As for the quantum emitters, we assume that they are characterized by two parameters — the resonant frequency ϵ and magnitude $|\boldsymbol{\mu}_i|$ of their transition dipole moment — and that they have fixed positions $\boldsymbol{R}_i$ and directions of their dipoles $\boldsymbol{\mu}_i/|\boldsymbol{\mu}_i|$. Hamiltonian for the QEs before introducing interactions is $H_{\rm QE} = \sum_i \hbar\epsilon(\hat{S}_i^z + \frac{1}{2})$ and its dipole moment operator

$$\hat{\boldsymbol{\mu}}_i = \boldsymbol{\mu}_i(\hat{S}_i^+ + \hat{S}_i^-). \tag{4}$$

Their dipoles interact with the resonator's electric field via the term

$$H_{\rm res\text{–}QE} = -\sum_i \hat{\boldsymbol{\mu}}_i \cdot \hat{\boldsymbol{E}}(\boldsymbol{R}_i) \tag{5}$$

and with each other via the quasistatic dipole–dipole interaction

$$H_{\rm QE\text{–}QE} = \frac{1}{4\pi\varepsilon_0} \sum_{i<j} \left(\frac{\hat{\boldsymbol{\mu}}_i \cdot \hat{\boldsymbol{\mu}}_j}{|\boldsymbol{R}_i - \boldsymbol{R}_j|^3} - 3\frac{[\hat{\boldsymbol{\mu}}_i \cdot (\boldsymbol{R}_i - \boldsymbol{R}_j)][\hat{\boldsymbol{\mu}}_j \cdot (\boldsymbol{R}_i - \boldsymbol{R}_j)]}{|\boldsymbol{R}_i - \boldsymbol{R}_j|^5} \right).$$

Finally, we take $H = H_{\rm res} + H_{\rm QE} + H_{\rm QE\text{–}QE} + H_{\rm res\text{–}QE}$ and perform the rotating wave approximation, dropping all the terms containing $\hat{b}_\lambda \hat{S}_i^-$, $\hat{b}_\lambda^\dagger \hat{S}_i^+$, $\hat{S}_i^- \hat{S}_j^-$ or $\hat{S}_i^+ \hat{S}_j^+$, obtaining

$$\begin{aligned} H = &\sum_\lambda \hbar\omega_\lambda \hat{b}_\lambda^\dagger \hat{b}_\lambda + \sum_i \hbar\epsilon \left(\hat{S}_i^z + \frac{1}{2} \right) + \sum_{i,\lambda} V_{i\lambda}(\hat{b}_\lambda^\dagger \hat{S}_i^- + \hat{S}_i^+ \hat{b}_\lambda) \\ &+ \sum_{i<j} g_{ij}(\hat{S}_i^+ \hat{S}_j^- + \hat{S}_j^+ \hat{S}_i^-), \end{aligned} \tag{6}$$

with the coupling coefficients

$$V_{i\lambda} = \sqrt{\frac{\hbar\omega_\lambda}{2U_\lambda\varepsilon_0}} \boldsymbol{\mu}_i \cdot \boldsymbol{E}_\lambda(\boldsymbol{R}_i)$$

and

$$g_{ij} = \frac{1}{4\pi\varepsilon_0} \left(\frac{\hat{\boldsymbol{\mu}}_i \cdot \hat{\boldsymbol{\mu}}_j}{|\boldsymbol{R}_i - \boldsymbol{R}_j|^3} - 3\frac{[\hat{\boldsymbol{\mu}}_i \cdot (\boldsymbol{R}_i - \boldsymbol{R}_j)][\hat{\boldsymbol{\mu}}_j \cdot (\boldsymbol{R}_i - \boldsymbol{R}_j)]}{|\boldsymbol{R}_i - \boldsymbol{R}_j|^5} \right).$$

For practical calculations, it is usually not necessary to take into account all the resonator modes: only the modes with frequencies near enough to the resonant frequency of the QEs will significantly affect the system. Assuming there is only one such significant mode (which is also the assumption of the Dicke model), we arrive at the Hamiltonian (1).

The RWA allows for a decomposition of the Hilbert space into subspaces defined by their excitation number N and the Hamiltonian (6) can then be easily defined only on those subspaces. The dimensionality $D(K, B, N)$ of such a subspace for a general case of B bosonic modes and K two-level systems is

$$D(K, B, N) = \sum_{\nu=0}^{N} \binom{K}{N-\nu} \binom{\nu + B - 1}{\nu},$$

as can be found using elementary combinatorics. Comparing this with the binomial identity gives an upper estimate $D(K, B, N) \leq (K + B + N - 1)^N / N!$, therefore for low excitation numbers, this makes it feasible to perform exact diagonalization of the Hamiltonian in this subspace even for quite large number of emitters and bosonic modes [the memory required for representing a nonsparse operator in such a subspace is proportional to $D(K, B, N)^2$ and the usual matrix diagonalization algorithms will have time complexity of about $O(D(K, B, N)^3)$; for $N = 1$, this allows for having hundreds of emitters on a workstation with a gigabyte of RAM].

3. The Scattering Approach

In the following, we compare the results of our model explained above to a multiple-scattering model described in Refs. 4 and 23. For details, we refer the reader to the supplement of Ref. 4, but we outline the main properties of the model here.

The approach is based on macroscopic quantum electrodynamics, where medium (including the plasmonic resonator in our case) is modeled by a continuum of harmonic oscillators coupled to the microscopic electromagnetic fields in a manner that (before quantization) reproduces the phenomenological constitutive relations; the electromagnetic field operators can be then expressed in terms of the classical dyadic Green's functions.[10] Adding the microscopic QEs and coupling them to these quantized fields gives rise to a Lippmann–Schwinger equation which is hard to solve if the QEs are two-level systems. Therefore, the two-level systems are approximated by harmonic oscillators, at the cost of reliability of the model for problems that involve multiple excitations. For a given initial state, e.g., some of the emitters excited, we can derive a light spectrum that can be detected in an arbitrary point of space.

In contrast to our model described in the previous section, this approach has some advantages: it gives the light spectrum — a quantity of direct experimental relevance, it accounts for the absorption in the media, and it includes the field retardation effects, keeping its validity at longer-than-wavelength scales. These features make it a good benchmark for our model. On the other hand, the multiple-scattering

approach will fail to describe the effects of higher level of excitation and it is significantly slower computationally, as it requires solving a separate matrix inversion problem for each sample frequency of the outgoing light spectrum, each inversion having the same time complexity as one exact diagonalization.

The multiple-scattering approach relies on the knowledge of the classical Green's function of the system in which the quantum emitters are located. In the following, we consider a medium consisting of a spherical nanoparticle in a homogeneous background. The classical dyadic Green's function for such system can be (for points outside the sphere) expressed as a sum of a free propagation part (equal to the Green's function of a homogeneous medium with wavenumber k_ω) and a part due to the scattering on the sphere, accounting for the field enhancement and Ohmic losses:

$$\boldsymbol{G}(\omega, \boldsymbol{r}, \boldsymbol{r}') = \boldsymbol{G}_0(\omega, \boldsymbol{r}, \boldsymbol{r}') + \boldsymbol{G}_{\text{scat}}(\omega, \boldsymbol{r}, \boldsymbol{r}'),$$

where the latter can be expanded into a Mie series:

$$\boldsymbol{G}_{\text{scat}}(\omega, \boldsymbol{r}, \boldsymbol{r}') = \frac{ik_\omega}{4\pi} \sum_{lm} c_{lm} \Big[\rho_l^{\text{mg.}} \boldsymbol{M}_{lm}^{(1)}(k_\omega \boldsymbol{r}) \otimes \boldsymbol{M}_{lm}^{(1)*}(k_\omega \boldsymbol{r}') \times \rho_l^{\text{el.}} \boldsymbol{N}_{lm}^{(1)}(k_\omega \boldsymbol{r}) \otimes \boldsymbol{N}_{lm}^{(1)*}(k_\omega \boldsymbol{r}') \Big], \tag{7}$$

where $\boldsymbol{M}_{lm}^{(1)}, \boldsymbol{N}_{lm}^{(1)}$ are the regular transverse vector spherical wavefunctions, $\rho_l^{\text{mg.}}$, $\rho_l^{\text{el.}}$ are the Mie reflection coefficients and c_{lm} is a normalization factor depending on the convention used for the spherical wavefunctions. Detailed expressions for calculating $\boldsymbol{G}_{\text{scat}}$ can be found in Ref. 20.

4. Comparison

Let us take a simple physical system in order to compare our modified Dicke model and the multiple-scattering approach. The system consists of a metal nanosphere, and several molecular dipoles modeled as two-level systems nearby, as in Fig. 1. The relative permittivity of the nanosphere is approximated by the Drude model, $\varepsilon(\omega) = \varepsilon_\infty - \frac{\omega_p^2}{\omega(\omega + i\gamma_p)}$ with parameters $\varepsilon_\infty = 4.6$ and $\hbar\gamma_p = 0.001$ eV (this parameter is chosen arbitrarily low in order to create peaks comparable to the modified Dicke model spectrum), its radius is $r = 7$ nm, and we vary its plasma frequency ω_p. In the quasistatic approximation,[15] lth-order electric multipole resonances of a nanosphere are determined by the equation: $0 = \varepsilon(\omega_l) + \varepsilon_b(l+1)/l$ where ε_b is the environment relative permittivity, which we set to one for the comparison. In our case, the dipole resonance is thus located at $\omega_1 = 3.02$ eV$/\hbar$ — we use this value as the mode frequency ω in the Hamiltonian (1), whereas for the multiple-scattering method, we use Mie theory with the aforementioned parameters to calculate the nanosphere response.

The molecules have transition dipole moments of $|\boldsymbol{\mu}| = 0.19$ eV $\cdot$ nm, they are aligned in the z-direction and positioned in a plane 8 nm from the center of the

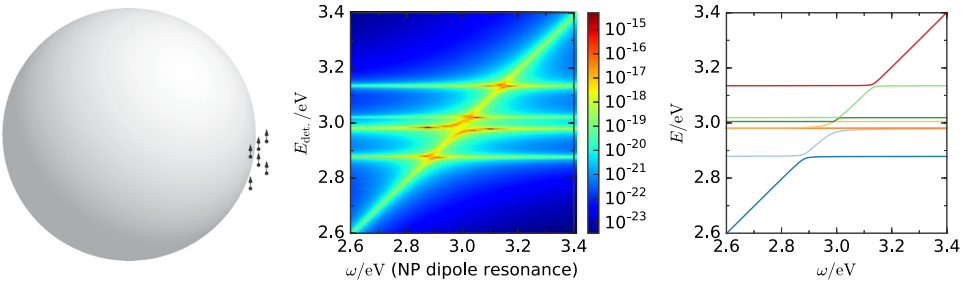

Fig. 1. (Color online) (a) Configuration of the system with six QEs and the corresponding spectra, varying the plasma frequency of the metal: (b) far-field light spectra obtained by the multiple-scattering method and (c) eigenvalues of the Hamiltonian (1). Both in (b) and (c) only the electric z-dipole part of the nanoparticle response is considered.

nanosphere. These values were chosen in order to make the molecular interactions significant. For simplicity and clarity of the figures, we include only the electric dipole response $\rho_1^{\mathrm{el.}}$ of the nanosphere, neglecting all the higher multipole terms in the calculation of the Green's functions used in the multiple-scattering model (7). In our modified Dicke model, we assume that the field has the same shape as it would have in the electrostatic case of a polarized sphere, i.e., we neglect the outward radiation. Moreover, here we place the molecules near the equatorial plane perpendicular to the z-axis in order to keep the interactions of the x and y dipoles of the nanoparticle negligible. Therefore, we can model the system with the Hamiltonian (1) [otherwise the more general Hamiltonian (6) would be needed].

In Fig. 1 we show the light spectra obtained by the multiple-scattering method at a point located 10 μm away from the center of the nanoparticle together with the eigenenergies obtained from our model. There is a clear correspondence between the peaks of the light spectra and the eigenenergies from the respective approaches. However, not every energy level has its corresponding peak in the light spectra; we discuss these dark states in the next section.

The presented approach can be generalized to multiple bosonic modes in a straightforward manner. In Fig. 2 we show the spectra for the same configuration as in Fig. 1, but now with higher multipole modes of the nanoparticle included for both models — they appear as additional terms in the Green's function expansion (7) of the multiple-scattering model, and as additional quasistatic electric multipole modes included into the bosonic part of the Hamiltonian in the modified Dicke model (see Appendix A). The higher multipoles significantly affect the part of the spectra that is above the nanoparticle dipole resonance if the QEs are placed close enough to the nanoparticle, as they provide additional channels through which the QEs can indirectly interact, and many new states appear near the planar surface plasmon–polariton frequency. This nanoparticle-mediated interaction is present in both models, determined either by the interaction coefficients $V_{i\lambda}$ or by

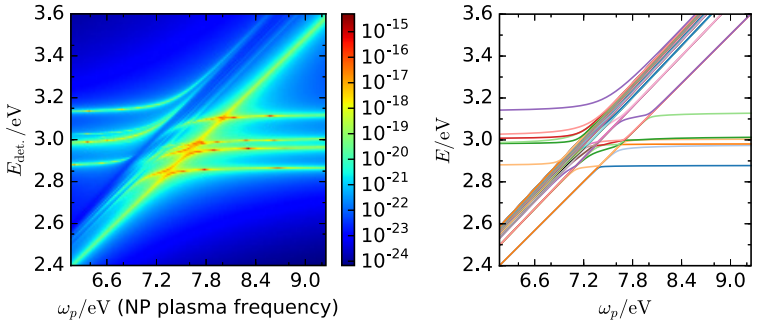

(a) (b)

Fig. 2. (Color online) Spectra corresponding to the configuration from Fig. 1, here with higher multipole effects of the nanoparticle included (up to $l = 20$), varying the plasma frequency of the metal: (a) far-field light spectra obtained by the multiple-scattering method and (b) eigenvalues of the Hamiltonian (6).

the scattering part of the Green's function $\boldsymbol{G}_{\mathrm{scat}}$, and as Fig. 1 demonstrates, has very similar effects on the shape of the spectra. As the focus of our current study are the dipole–dipole interactions between the QEs rather than a detailed analysis of the QE–nanoparticle couplings and nanoparticle mode structure, we neglect the higher multipoles in the rest of this section, keeping only the nanoparticle's dipole modes in both models.

4.1. *Characterization of the dark modes*

Hamiltonian (1) describes a closed quantum system of electric dipoles with Coulombic interaction and certain internal dynamics, and by itself does not carry any information about interaction with radiation, hence nor about the visibility of its eigenstates. Therefore, we extend the system to include radiation modes and assess their visibility using perturbation theory. Let the new Hamiltonian be

$$H' \equiv H_0 + V = H + \sum_{\underline{\boldsymbol{k}}} \hbar\omega_{\boldsymbol{k}} a^\dagger_{\underline{\boldsymbol{k}}} a_{\underline{\boldsymbol{k}}} + V_{\mathrm{ext}}, \tag{8}$$

where $\underline{\boldsymbol{k}} \equiv (\boldsymbol{k}, \iota)$ labels the transversal (radiation) modes with mutually orthogonal wave and polarization vectors $\boldsymbol{k}$ and $\boldsymbol{\varepsilon}_{\boldsymbol{k},\iota}$ (here $\iota = 1, 2$ labels the polarization basis vectors), $\omega_{\boldsymbol{k}} = c|\boldsymbol{k}|$ is the corresponding mode frequency and V_{ext} is the interaction between the transversal modes and all the dipoles (including the nanoparticle):

$$V_{\mathrm{ext}} = -\hat{\boldsymbol{E}}^{\perp}(\boldsymbol{r} = 0) \cdot \hat{\boldsymbol{\mu}}_{\mathrm{tot.}} \tag{9}$$

$$= \sum_{\underline{\boldsymbol{k}}} i\sqrt{\frac{\hbar\omega_{\boldsymbol{k}}}{2\varepsilon_0 L^3}} (\boldsymbol{\varepsilon}_{\underline{\boldsymbol{k}}} a_{\underline{\boldsymbol{k}}} - \boldsymbol{\varepsilon}_{\underline{\boldsymbol{k}}} a^\dagger_{\underline{\boldsymbol{k}}}) \cdot \left(\boldsymbol{\mu}_{\mathrm{NP}}(b + b^\dagger) + \sum_i \boldsymbol{\mu}_i (S_i^+ + S_i^-) \right). \tag{10}$$

Here we use the usual way to quantize transversal EM modes.[3] We note that the transversal modes are orthogonal to the electric field of the resonator quasistatic

modes, as these are fully longitudinal. Furthermore, we assume a cutoff in the frequencies such that $\boldsymbol{k} \cdot \boldsymbol{r}_{\text{sys}} \ll 1$ where $\boldsymbol{r}_{\text{sys}}$ is the radius of the volume in which the dipoles are placed, so all the dipole positions can be replaced with $\boldsymbol{r} = 0$ (dipole approximation for the whole original system) and ultraviolet divergences are avoided. Finally, we assume that all the conditions to apply the Fermi's golden rule are fulfilled. Decay rate of an initial state $|\alpha\rangle$ from the eigenspace of the original Hamiltonian H into the continuum of final transversal photonic states $|f\rangle$ is proportional to the sum of squares of the corresponding transition amplitudes[3]:

$$\Gamma_\alpha \propto \sum_f |\langle f|V_{\text{ext}}|\alpha\rangle|^2. \tag{11}$$

To keep the length of the formulae reasonable, in the following we denote $\boldsymbol{\mu}_0 \equiv \boldsymbol{\mu}_{\text{NP}}$ and $S_0^+ \equiv b^\dagger$ and $S_0^- \equiv b$. In the single excitation subspace (using RWA), both initial and final subspaces are spanned by the states obtained by applying a single corresponding creation operator onto the vacuum state of H_0, $|f\rangle = |\underline{\boldsymbol{k}}\rangle \equiv a^\dagger_{\underline{\boldsymbol{k}}}|0\rangle$ and $|\alpha\rangle = \sum_{i=0}^K c_i S_i^+|0\rangle$. Substituting this to (11) gives

$$\begin{aligned}
\Gamma_\alpha \propto & \sum_{\underline{\boldsymbol{k}}} \langle\alpha|\hat{\boldsymbol{\mu}}_{\text{tot.}} \cdot \sum_{\underline{\boldsymbol{k}}'} i\sqrt{\frac{\hbar\omega_{\boldsymbol{k}'}}{2\varepsilon_0 L^3}}(\boldsymbol{\varepsilon}_{\underline{\boldsymbol{k}}'} a_{\underline{\boldsymbol{k}}'} - \boldsymbol{\varepsilon}_{\underline{\boldsymbol{k}}'} a^\dagger_{\underline{\boldsymbol{k}}'}) a^\dagger_{\underline{\boldsymbol{k}}} \\
& \times |0\rangle\langle 0| a_{\underline{\boldsymbol{k}}} \sum_{\underline{\boldsymbol{k}}''} -i\sqrt{\frac{\hbar\omega_{\boldsymbol{k}''}}{2\varepsilon_0 L^3}} \left(\boldsymbol{\varepsilon}_{\underline{\boldsymbol{k}}''} a_{\underline{\boldsymbol{k}}''} - \boldsymbol{\varepsilon}_{\underline{\boldsymbol{k}}''} a^\dagger_{\underline{\boldsymbol{k}}''}\right) \cdot \hat{\boldsymbol{\mu}}_{\text{tot.}}|\alpha\rangle \\
= & -\sum_{\underline{\boldsymbol{k}}} \frac{\hbar\omega_{\boldsymbol{k}}}{2\varepsilon_0 L^3} \langle\alpha|\hat{\boldsymbol{\mu}}_{\text{tot.}} \cdot \boldsymbol{\varepsilon}_{\underline{\boldsymbol{k}}} a_{\underline{\boldsymbol{k}}} a^\dagger_{\underline{\boldsymbol{k}}}|0\rangle\langle 0| a_{\underline{\boldsymbol{k}}} a^\dagger_{\underline{\boldsymbol{k}}} \boldsymbol{\varepsilon}_{\underline{\boldsymbol{k}}} \cdot \hat{\boldsymbol{\mu}}_{\text{tot.}}|\alpha\rangle.
\end{aligned}$$

Here we used the commutativity of the photonic operators $a_{\underline{\boldsymbol{k}}}, a^\dagger_{\underline{\boldsymbol{k}}}$ with the $S_i^\pm$ operators contained in $\hat{\boldsymbol{\mu}}_{\text{tot.}}$ together with the fact that $a_{\underline{\boldsymbol{k}}} a_{\underline{\boldsymbol{k}''}}|\alpha\rangle = 0$ and $\langle 0|a_{\underline{\boldsymbol{k}}} a^\dagger_{\underline{\boldsymbol{k}''}}|0\rangle$ is nonzero only if $\underline{\boldsymbol{k}''} = \underline{\boldsymbol{k}}$. We assume that the space supporting the radiation modes is spherically symmetric, hence for the sum over $\underline{\boldsymbol{k}}$ we get

$$\begin{aligned}
\sum_{\underline{\boldsymbol{k}}} \omega_{\boldsymbol{k}} \boldsymbol{\varepsilon}_{\underline{\boldsymbol{k}}} a_{\underline{\boldsymbol{k}}} a^\dagger_{\underline{\boldsymbol{k}}}|0\rangle\langle 0| a_{\underline{\boldsymbol{k}}} a^\dagger_{\underline{\boldsymbol{k}}} \boldsymbol{\varepsilon}_{\underline{\boldsymbol{k}}} &= \sum_{\underline{\boldsymbol{k}}} \omega_{\boldsymbol{k}} \boldsymbol{\varepsilon}_{\underline{\boldsymbol{k}}}|0\rangle\langle 0|\boldsymbol{\varepsilon}_{\underline{\boldsymbol{k}}} \\
&= |0\rangle\langle 0| \sum_k \omega_k \sum_{\iota=1,2} \int d\Omega\, \boldsymbol{\varepsilon}_{\boldsymbol{k},\iota} \boldsymbol{\varepsilon}_{\boldsymbol{k},\iota} \\
&= \frac{8}{3}\pi \boldsymbol{I}|0\rangle\langle 0| \sum_k \omega_k,
\end{aligned}$$

i.e., a multiple of the unit tensor $\boldsymbol{I}$ (one way to calculate the angular integral $\int d\Omega \boldsymbol{\varepsilon}_{\boldsymbol{k},\iota} \boldsymbol{\varepsilon}_{\boldsymbol{k},\iota}$ in the last step is to choose the unit vectors tangential to the circles of latitude and longitude for the polarization vectors: $\boldsymbol{\varepsilon}_{\boldsymbol{k},1} = \hat{\boldsymbol{\theta}}, \boldsymbol{\varepsilon}_{\boldsymbol{k},2} = \hat{\boldsymbol{\phi}}$). Therefore,

$$\begin{aligned}\Gamma_\alpha &\propto \langle 0| \left(\sum_{i=0}^{K} c_i^* S_i^- \right) \sum_{j=0}^{K} \boldsymbol{\mu}_j (S_j^+ + S_j^-)|0\rangle \\ &\quad \times \langle 0| \sum_{m=0}^{K} \boldsymbol{\mu}_m (S_m^+ + S_m^-) \sum_{n=0}^{K} c_n S_n^+ |0\rangle \\ &= \langle 0| \sum_{i=0}^{K} c_i^* S_i^- \sum_{j=0}^{K} \boldsymbol{\mu}_j S_j^+ |0\rangle \cdot \langle 0| \sum_{m=0}^{K} \boldsymbol{\mu}_m S_m^- \sum_{n=0}^{K} c_n S_n^+ |0\rangle. \end{aligned} \tag{12}$$

All the nonzero terms of expressions on the sides of the projector $|0\rangle\langle 0|$ are just multiples of the vacuum state, so the projector can be put away,

$$\Gamma_\alpha \propto \langle \alpha| \sum_{j=0}^{K} S_j^+ \boldsymbol{\mu}_j \cdot \sum_{m=0}^{K} S_m^- \boldsymbol{\mu}_m |\alpha\rangle \equiv \langle \alpha| \hat{P} |\alpha\rangle.$$

The radiative decay rates are thus up to a constant factor given by the expectation value of an observable $\hat{P}$. The operator

$$\hat{P} = \sum_{j=0}^{K} S_j^+ \boldsymbol{\mu}_j \cdot \sum_{m=0}^{K} S_m^- \boldsymbol{\mu}_m \tag{13}$$

resembles the total dipole moment squared, but it is not equal to the operator $\hat{\boldsymbol{\mu}}_{\text{tot.}}^2 = \hat{\boldsymbol{\mu}}_{\text{tot.}} \cdot \hat{\boldsymbol{\mu}}_{\text{tot.}}$ which contains a positive offset caused by the presence of terms like $S_j^- S_j^+$, causing an overall positive shift and therefore its expectation value being always positive. On the other hand, $\langle \alpha|\hat{P}|\alpha\rangle$ can be zero, which means that the state $|\alpha\rangle$ does not radiate (in the given approximation), i.e., it is a dark state. Directly evaluating the operators acting on the vacuum states in (12), it can also be seen that $\langle \alpha|\hat{P}|\alpha\rangle = |\sum_{i=0}^{K} c_i \boldsymbol{\mu}_i|^2$, so in fact the operator $\hat{P}$ is analogous to the *classical sense* of the square of total dipole moment rather than the square of the *total dipole moment quantum operator*.

Figures 3(c)–3(e) and 3(f) show the expectation values $\langle \alpha|\hat{P}|\alpha\rangle$ for the eigenstates of H in the example configurations depicted in Fig. 3(a) for two different values of the QE transition dipole moment. Those states for which the expectation value is very low are indeed dark also in the results of the multiple-scattering method. Moreover, the relative intensities of the brighter states correspond well to each other, $S(\alpha)/S(\beta) \approx \langle \alpha|\hat{P}|\alpha\rangle / \langle \beta|\hat{P}|\beta\rangle$, if the compared eigenstates $|\alpha\rangle, |\beta\rangle$ are well separated from others (otherwise their contributions in the total light spectrum cannot be distinguished) and if they do not contain significant contribution from the nanoparticle dipole (the emission properties of the two types of dipoles differ because of the different internal loss channels, which are however not considered in our model). This is demonstrated in Fig. 3(i) where the QEs are further away from the nanoparticle than in the other examples and they are all very close to each other, so their mutual dipole–dipole couplings g_{ij} are stronger than their couplings with the nanoparticle V_i.

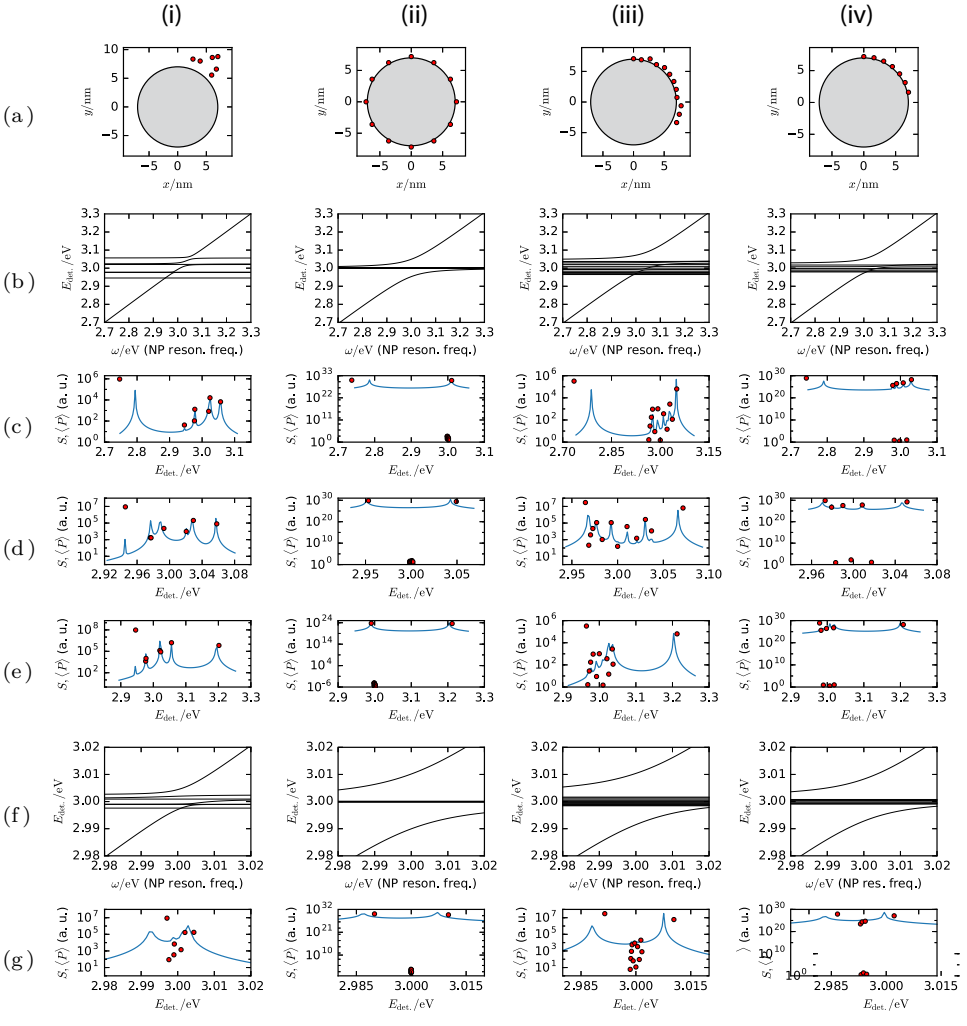

Fig. 3. (Color online) (a) Example configurations of quantum emitters in the equatorial plane of a spherical nanoparticle (with dipoles oriented perpendicular to the plane), (b) the corresponding energy spectra obtained from the modified Dicke model for varying nanoparticle resonance and light spectra from the multiple-scattering model (blue lines, arbitrary units) together with the expectation values of the observable $\hat{P}$ for the energy eigenstates (red dots, arbitrary units) for the nanoparticle dipole resonance set at (c) 2.8 eV, (d) 3.0 eV and (e) 3.2 eV. The single QEs have transition energy $\hbar\epsilon = 3.0$ eV and dipole moment [panels (c)–(e)] $\mu = 0.19$ eV $\cdot$ nm $= 9.1$ D; the Drude damping is set to $\hbar\gamma_P = 1$ meV. Rows (f) and (g) are analogous to rows (b) and (d) but for a lower dipole moment $\mu = 0.04$ eV $\cdot$ nm $= 1.9$ D.

5. Exact Diagonalization Results

In this section, we vary the parameters of the model Hamiltonian (1) in a systematic way and compute the energy spectrum by exact diagonalization. Again, we focus only on the single excitation subspace, i.e., the energy eigenstates satisfying $N = 1$.

Such states can be expressed in the form $|\psi\rangle = (C\hat{b}^\dagger + \sum_i c_i \hat{S}_i^+)|g\rangle$ where c_i, C are still complex coefficients.

Here we use a different way of determining V_i than in the benchmark calculation above. We assume that the mode field is homogeneous in the volume of interest (where the QEs are), with the intensity $\boldsymbol{E}$ being one of the parameters. The coupling constants are again determined as $V_i = -\boldsymbol{\mu}_i \cdot \boldsymbol{E}$ and are therefore dependent mainly on the orientation of a given dipole.

In the following, we study the energy spectra for varying energy ω of the bosonic field, keeping the free TLS energy difference ϵ fixed. This captures the possibility to tune the field mode, whereas the spectral properties of a molecule are given. A sample spectrum is shown in Fig. 4. Regardless of the specific configuration, in the single excitation subspace there will generally be a bounded "band" of $K-2$ eigenvalues (where K is the number of QEs) nearby the original ϵ, and two "polariton branches" below and above the band asymptotically approaching ω for $\omega \ll \epsilon$ and $\omega \gg \epsilon$, respectively. The exact positions of the eigenvalues inside the band depend nontrivially on the configuration of the dipoles, but there are several quantitative attributes of the shape of the spectra — e.g., the position and the width of the band or the separation of the polariton branches — whose dependence on some basic parameters can be studied statistically.

Some observations about the spectra follow directly from the structure of the Hamiltonian (1). For small values of V_i, the width of the central band in the spectra is directly proportional to the dipole–dipole couplings g_{ij}. Therefore the width scales with the dipole moment as μ^2 and with the length scale l (proportional to the interparticle distances) as l^{-3}, and hence it grows linearly with the concentration of the molecules if the other parameters stay fixed. When the dipole–dipole couplings

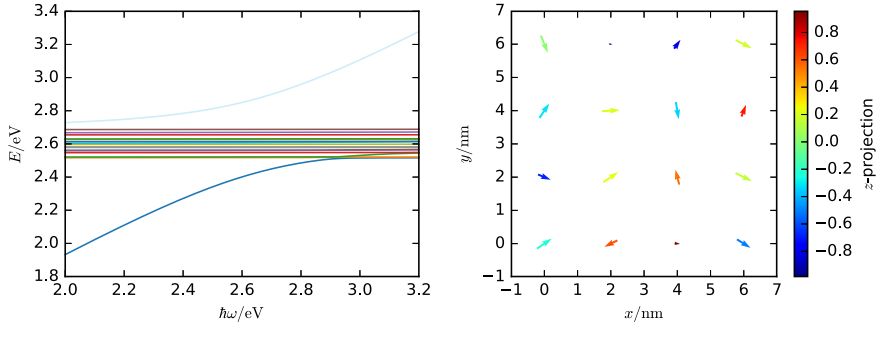

(a) (b)

Fig. 4. (Color online) (a) Sample configuration of the dipoles and (b) the corresponding energy spectrum of the single excitation subspace of the modified Dicke model, with varying energy of the bosonic mode. The parameters used here are $E = E_z = 2.4 \cdot 10^8$ V $\cdot$ m^{-1}, $\epsilon = 2.6$ eV$/\hbar$ and $\mu = 20$ D. Here the dipoles are located in a regular 4×4 square lattice but are randomly oriented. Two main polariton branches appear together with a central band of energies around the original transition frequency of a single molecule. The width of the central band grows with the dipole–dipole couplings g_{ij}.

g_{ij} are large enough, the lower polariton branch might cross some of the central band energies for $\omega > \epsilon$, as can be seen in Fig. 4.

The magnitude of the dipole–field couplings V_i then affects mainly the mutual separation of the polariton branches. For small enough dipole–dipole couplings g_{ij} (so that the band stays well between the polariton branches) the lower polariton branch approaches ϵ for large ω, whereas there is a certain gap between the upper branch and ϵ for small ω. We observe that the computed polariton branches fit quite well onto the formula

$$\tilde{\omega}_{\pm}^2 = \frac{1}{2}\left[\omega^2 + {\omega_0}^2 + \Omega^2 \pm \sqrt{\left(\omega^2 + {\omega_0}^2 + \Omega^2\right)^2 - 4\omega^2\omega_0^2}\right]. \tag{14}$$

Such a dependence is found in the dispersion relations derived from several models of propagating waves (e.g., surface plasmon polaritons[22] or usual electromagnetic plane waves[11]) interacting with emitters distributed homogeneously in the direction of wave propagation and without dipole–dipole interactions. In that context, ω from (14) is the frequency of the wave of a particular wavelength in the absence of the emitters, ω_0 is the transition frequency of the uncoupled emitters and Ω^2 is a quantity linearly proportional to the polarizability of the emitters and also to their concentration; Ω is the Rabi splitting, equal to the difference between the polariton branches $\tilde{\omega}_+ - \tilde{\omega}_-$ at resonance ($\omega = \omega_0$), and $\sqrt{\omega_0^2 + \Omega^2}$ corresponds to the low-energy asymptote of the upper polariton branch.

For larger g_{ij}, the lower polariton branch starts to cross some of the band levels and therefore fitting the lowest eigenvalue onto $\tilde{\omega}_-$ is no longer reliable. Nevertheless, using only the upper branch for the fit yields still reliable results even for ω_0. As could be seen in Figs. 3(i), 3(iii) and 3(iv), the shape of the lower polariton branch may still be apparent in the spectrum of the Hamiltonian even if it penetrates the central band.

In the following, we will see that neither of the parameters ω_0, Ω depend significantly on the dipole–dipole couplings g_{ij} (cf. Sec. 5.2 and Fig. 7). The polariton splitting Ω does, however, scale with the single emitter dipole moment magnitude μ and the number of dipoles N as $\Omega \propto \sqrt{\mu^2 N}$. Therefore, the width of the central band will grow faster than the polariton splitting when the dipole concentration is increased.

5.1. *Effects due to randomness*

As mentioned in Sec. 1, the QEs in the nanoplasmonic system are usually distributed randomly near the metallic structures, having also random directions. In order to capture the effects of the randomness, we performed statistical simulations with varying degree of randomness in angular and positional configurations of the QEs. In both cases, we start with a rectangular array of dipoles aligned in a single direction (which corresponds to the direction of the field intensity).

We choose several statistics calculated from the resulting spectra. The width of the band can be described in multiple ways, one of them is the difference Δ_f

between the second highest and the second lowest eigenvalues at $\omega = \epsilon$. The average ϵ_m of these two eigenvalues characterizes the position of the band. For each sample, we perform a least-square fit of the spectra onto the dispersion function (14) in order to obtain the parameters ω_0 and Ω, which show the asymptotic behavior of the polariton branches and their splitting.

As for the directions, the randomness is parameterized by the maximum deviation polar angle Θ. Each dipole is rotated from its aligned direction by a random polar angle θ chosen between 0 and Θ such that $\cos\theta$ has uniform distribution between $\cos\Theta$ and 1 and the azimuth angle of the rotation is always chosen uniformly from all directions; therefore the dipole moment vector is uniformly distributed on the spherical surface delimited by the maximum polar angle Θ. The resulting distributions of Δ_f and Ω are illustrated in Fig. 5 for a 4×4 square array with 2 nm space separation with two different magnitudes of dipole moment, 2 D and 15 D.

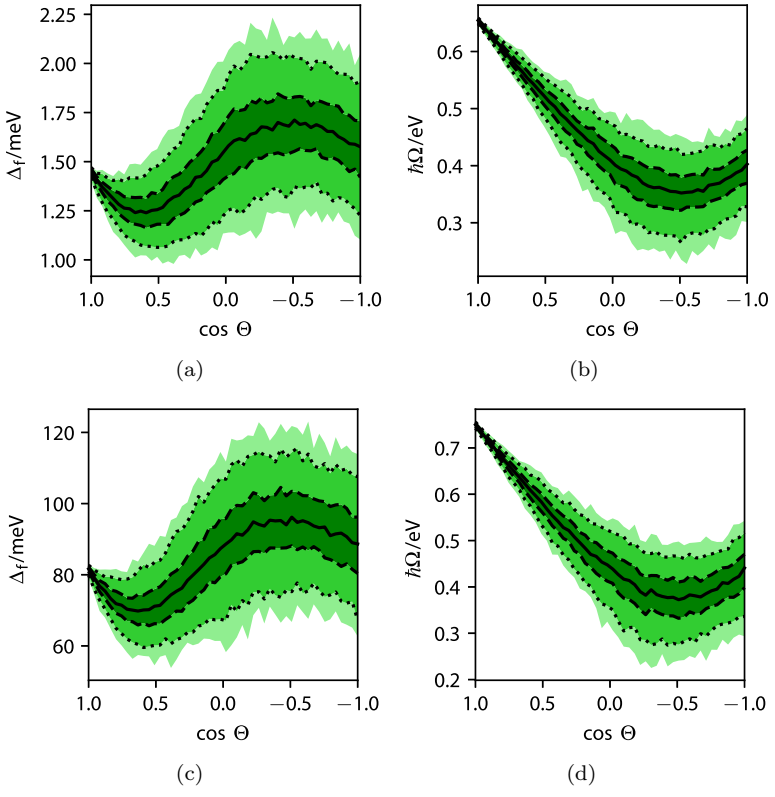

Fig. 5. (Color online) Effects of angular randomness on the spectrum in a 4×4 dipole array (16 nm $\times$ 16 nm): (a), (c) widths of the dipole band Δ_f taken as the difference between the second highest and the second lowest eigenvalue at $\omega = \epsilon = 2.6$ eV; (b), (d) polariton splittings Ω from fitting the relation (14). The parameters are (a), (c) $\mu = 2$ D, $E = E_z = 2.4 \cdot 10^9$ V $\cdot$ m^{-1} and (b), (d) $\mu = 15$ D, $E = E_z = 3.2 \cdot 10^8$ V $\cdot$ m^{-1} (in both cases $\mu E_z = 0.1$ eV). The lines correspond to the quantiles 0.01, 0.05, 0.25, 0.5, 0.75, 0.95 and 0.99, i.e., the areas delimited by light, medium and dark shades delimit 98%, 90% and 50% of the values, respectively.

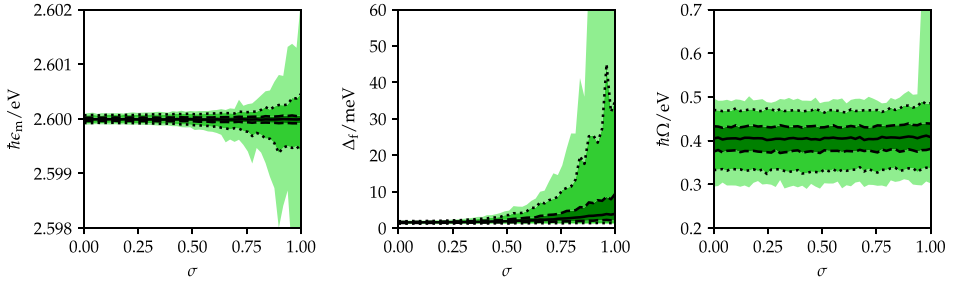

Fig. 6. (Color online) Effects of the position randomness on the spectrum in a 4×4 dipole array (16 nm $\times$ 16 nm) for $\mu = 2$ D and $E = E_z = 2.4 \cdot 10^9$ V $\cdot$ m^{-1}. The dipoles are displaced along each axis up to 1 nm. (a) Center of the dipole band taken as the mean of the second highest and the second lowest eigenvalues at $\omega = \epsilon = 2.6$ eV; (b) width of the dipole band Δ_f; and (c) polariton splitting Ω from fitting the relation (14). The lines correspond to the quantiles 0.01, 0.05, 0.25, 0.5, 0.75, 0.95 and 0.99, i.e., the areas delimited by light, medium and dark shades delimit 98%, 90% and 50% of the values, respectively.

The dipole–field couplings were however kept in the same range of ± 0.26 eV. In all cases, the band center ϵ_m was equal to the QE natural frequency ϵ with a relative error less than $2 \cdot 10^{-4}$. The fitted value of ω_0 was equal to ϵ with 1% accuracy (although always below the prescribed ϵ).

The bandwidth depends mainly on the magnitude of the dipole moment, $\Delta_f \propto \mu^2$. The directional randomness causes variation in the bandwidth, which in extreme cases can differ by about a factor of two for different samples.

Next, we added some noise into the dipoles' positions. The initial configuration was a 4×4 square array of randomly oriented dipoles, with $a = 2$ nm distance between dipoles. However, a random offset from the interval $(-\sigma a/2, \sigma a/2)$ was then added to each Cartesian coordinate of each dipole, where σ is a randomness parameter. The resulting distributions of selected statistics (for $\mu = 2$ D) are shown in Fig. 6.

The effect of the dipole configuration on the band position is again negligible as it stays within a 1 meV range around the original ϵ in 90% of the cases for the maximally random case. However, the bandwidth might increase substantially for some fraction of samples in the maximally random case. This is caused by the fact that the distance between two neighboring dipoles can approach zero and thus their mutual coupling g_{ij} might become very large. As will be discussed later, this situation is mostly unphysical because of the nonzero size of the QEs. The value of Ω is apparently unaffected by the positions except for a very small fraction of cases, which again correspond to unrealistically small distances between the dipoles.

5.2. *Scaling effects*

In order to explore the effects of the direct dipole–dipole coupling of the QEs, we scaled the transition dipole moment relevant for the direct coupling while keeping

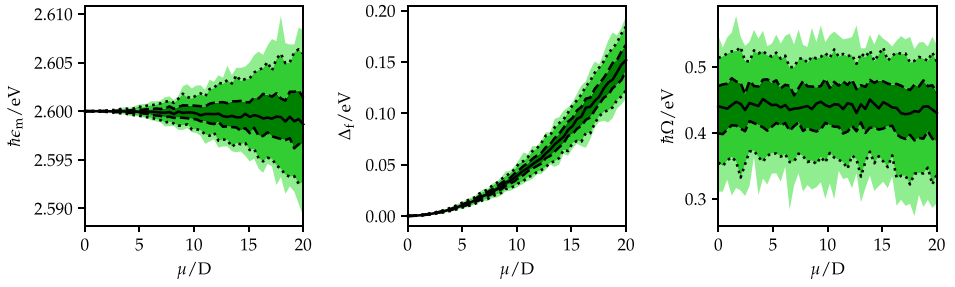

Fig. 7. (Color online) Scaling of the observed statistics with the transition dipole moment μ, keeping the maximum field–dipole couplings fixed at $V_i \leq \mu E_z = 0.1$ eV. Randomized are both dipole orientations and positions. The lines correspond to the quantiles 0.01, 0.05, 0.25, 0.5, 0.75, 0.95 and 0.99, i.e., the areas delimited by light, medium and dark shades delimit 98%, 90% and 50% of the values, respectively. Varying the molecular density n has the same effect as varying μ^2.

the magnitude of V_i coupling terms. As stated before, increasing μ by the factor of α is equivalent to reducing the intermolecular distance by the factor of $\alpha^{-2/3}$. The results for the scenario with the 4×4 array of QEs with fixed positions at 2 nm interparticle distance and fully random directions is shown in Fig. 7. As expected, the bandwidth Δ_f shows clear quadratic dependence on μ (thus linear dependence on g_{ij}). The band position remains well at the QE transition frequency ϵ. (Only the random fluctuations of the outermost energies of the band scale linearly with the bandwidth, which leads to the quadratic broadening of the Δ_f distribution with μ.) The polariton splitting Ω was found to be almost independent of dipole–dipole interactions. Hence μ influences the polariton splitting only via the $V_i \propto \boldsymbol{\mu}_i \cdot \boldsymbol{E}(\boldsymbol{r}_i)$ terms.

Because of the aforementioned equivalence of scaling dipole moments and intermolecular distances (thus concentrations), the results can be interpreted accordingly — for example in Fig. 6(b), we would get a linear dependence on QE concentrations instead of quadratic dependence of QE dipole moments.

6. Conclusions

Using a modified Dicke model, we have shown that significant direct couplings between two-level quantum emitter dipoles — which may result from their high concentration and high individual transition dipole moments — lead to new collective states with eigenenergies being split and shifted away from the original transition frequency of individual dipoles. Moreover, some of these states could be seen as significant peaks in the light spectrum radiated from the system; this can be attributed to the significant effective dipole moment that these states exhibit.

A question naturally follows as to whether the effects of the dipole–dipole interaction described above can be probed experimentally in the nanoplasmonic systems.

The Hamiltonian (1), due to all the simplifications made, describes a closed system without any coupling to a probing field. We have shown, however, that the dark states are characterized by very low expectation value of the observable P defined by Eq. (13).

The experiments showing the strong coupling between the plasmonic excitations and QEs are characterized by the observable polariton splitting. While increasing the number of QEs and their couplings to a plasmonic nanoparticle increases the polariton splitting, this does not require any direct dipole–dipole interactions between the QEs. We showed that if the dipole–dipole couplings between the QEs are present, the previously degenerate QE transition energies split into a broader band and some of the resulting states might radiate much more intensively than others. However, this requires really significant dipole–dipole coupling strengths. Larger dipole–dipole couplings can be attained by increasing the QE concentration and/or transition dipole moment. With a transition dipole moment $\mu \approx 10$ D and separations between the emitters of ≈ 1 nm, there should be an observable band containing highly radiant states, cf. Fig. 3(d), but such values might not be easy to attain. One of the most popular QEs used in active nanoplasmonic systems is the rhodamine 6G (R6G) dye. The number density of solid R6G is about[26] $1.6 \cdot 10^{21}$ cm^{-3}, corresponding to the intermolecular distance of 0.86 nm. The transition dipole moment of a separate R6G molecule is about[14] 2 D. These values correspond approximately to the parameters of Fig. 3(f), where we might still expect some of the effects to be observable. However, R6G is diluted or embedded into a polymer in the experiments. The number density of $2.5 \cdot 10^{19}$ cm^{-3} and typical intermolecular separation of 3.5 nm, corresponding to the saturated water solution of R6G,[25] thus provide a more realistic estimate. For such parameters, the dipole–dipole couplings are so small that no observable effects can be expected.

Based on these arguments, we can speculate that it would be challenging but not impossible to observe effects of the direct quantum emitter dipole–dipole couplings in the nanoplasmonic systems: it demands a high value of the dipole moment concentration. Also in the paper of Salomon *et al.*,[16] the new mode (analog of our bright modes but in a totally different geometry) appears in the absorption spectra for a high dipole moment value of 25 D and concentration of 10^{19} cm^{-3}. Note that here we studied only the single excitation subspace. It is possible that other important effects of the dipole–dipole interactions could take place for higher excitation numbers.

Appendix A. Electric Field of Spherical Quasistatic Modes

The quasistatic modes in a system consisting of parts, each of which is filled with a different homogeneous and isotropic medium, are obtained by solving Laplace's equation for the electrostatic potential, $-\Delta\phi = 0$, subjected to the corresponding interface conditions and constitutive relations. The electric field corresponding to this potential is given by $\boldsymbol{E} = -\nabla\phi$ and at the interface between media i and j,

Faraday's law leads to the condition $\boldsymbol{n}_{ij} \times (\boldsymbol{E}_j - \boldsymbol{E}_i) = 0$ where $\boldsymbol{n}_{ij}$ is the unit vector normal to the interface and $\boldsymbol{E}_j, \boldsymbol{E}_i$ are the respective limits of the electric field when approaching the given point on the boundary. If we treat all the charges as bounded, Gauss law yields the second condition $\boldsymbol{n}_{ji} \cdot (\varepsilon_i \boldsymbol{E}_i - \varepsilon_j \boldsymbol{E}_j) = 0$. In the quasistatic approximation, it is assumed that the speed of light is infinite, $c \to \infty$, hence there is no magnetic field and all dynamics comes from the local internal response of the medium, given (in the linear regime) by the dielectric function $\varepsilon = \varepsilon(\boldsymbol{r}, \omega)$.

In the case of a spherical particle with radius R, solutions ϕ_{lm} of the Laplace's equation are most conveniently found as products of radial functions and spherical harmonics[12]:

$$\phi_{lm}^{\text{in}}(r, \theta, \varphi) = \xi_{lm} r^l Y_l^m(\theta, \varphi),$$
$$\phi_{lm}^{\text{out}}(r, \theta, \varphi) = \eta_{lm} r^{-n-1} Y_l^m(\theta, \varphi),$$

where the finite-energy solutions consist of ϕ_{lm}^{in} inside the particle ($r \leq R$) and ϕ_{lm}^{out} outside ($r \geq R$). Continuity of the potential on the boundary sets the relation between the coefficients $\xi_{lm} = \eta_{lm} R^{-2n-1}$. Moreover, calculating $\boldsymbol{E}_{lm} = -\nabla \phi_{lm}$,

$$\begin{aligned} \boldsymbol{E}_{lm}^{\text{in}} &= -\sum_{lm} \xi_{lm} r^{l-1} \left[l Y_l^m \hat{\boldsymbol{r}} + \frac{\partial Y_l^m}{\partial \theta} \hat{\boldsymbol{\theta}} + \frac{1}{\sin\theta} \frac{\partial Y_l^m}{\partial \varphi} \hat{\boldsymbol{\varphi}} \right], \\ \boldsymbol{E}_{lm}^{\text{out}} &= -\sum_{lm} \eta_{lm} r^{-l-2} \left[(l+1) Y_l^m \hat{\boldsymbol{r}} + \frac{\partial Y_l^m}{\partial \theta} \hat{\boldsymbol{\theta}} + \frac{1}{\sin\theta} \frac{\partial Y_l^m}{\partial \varphi} \hat{\boldsymbol{\varphi}} \right], \end{aligned} \tag{A.1}$$

and applying the aforementioned interface relations at $r = R$ yields the condition on the internal and external dielectric functions,

$$\varepsilon_{\text{in}}(\omega_l) = -\left(\frac{l+1}{l} \right) \varepsilon_{\text{out}}(\omega_l),$$

which also determines the frequency of the lth-degree quasistatic multipole mode. For the nonlossy Drude model $\varepsilon_{\text{in}}(\omega) = \varepsilon_\infty - \omega_p^2/\omega^2$ with constant background permittivity ε_{out}, the frequencies are

$$\omega_l = \sqrt{\frac{\omega_p^2}{\varepsilon_\infty + \frac{l+1}{l} \varepsilon_{\text{out}}}}.$$

In order to plug the field modes into the quantum model, the classical electric intensities have to be related to the energy U stored in the electric field (in the quasistatic approximation, the magnetic part does not contribute) $U = \varepsilon_0 \int d^3\boldsymbol{r} \, |\boldsymbol{E}(\boldsymbol{r})|^2/2$. (Note that here we do not include polarization.) If we use a convention in which the spherical harmonics are orthonormal (but they might complex as well as real),

$$\int d\Omega \, Y_l^{m*} Y_{l'}^{m'} = \delta_{ll'} \delta_{mm'},$$

then for a particular pair of indices l, m the result for the energy is, using the relations above,

$$\begin{aligned} U_{lm} &= \frac{\varepsilon_0}{2} \int d\Omega \left(\int_0^R dr r^2 |\boldsymbol{E}_{lm}^{\text{in}}| + \int_R^\infty dr r^2 |\boldsymbol{E}_{lm}^{\text{out}}| \right) \\ &= \frac{\varepsilon_0}{2} [l R^{2l+1} |\xi_{lm}|^2 + (l+1) R^{-2l-1} |\eta_{lm}|^2] \\ &= \frac{\varepsilon_0}{2} (2l+1) R^{-2l-1} |\eta_{lm}|^2. \end{aligned}$$

Due to the orthogonality of the spherical harmonics, the modes are orthogonal in the sense that the total electric field energy U of a linear combination of solutions ϕ_{lm} is given by summing their respective contributions U_{lm}.

Due to the assumed linearity, the quasistatic modes can be treated as independent harmonic oscillators and the instantaneous values of $\eta_{lm}(t)$ as their "displacements." In such case, U_{lm} play the role of the oscillators' "potential energies," which are equal to the total oscillators' energies when η_{lm} reach their maxima. Using the expression for U_{lm} as the potential energy part of the quantized harmonic oscillator, setting ω_l as the frequency of the quantized harmonic oscillator and performing the usual canonical transformation to the creation and annihilation operators $\hat{b}_{lm}^\dagger, \hat{b}_{lm}$, we get the expression for the quantized displacement:

$$\hat{\eta}_{lm} = \sqrt{\frac{R^{2l+1}\omega_l \hbar}{\varepsilon_0 (2l+1)}} (\hat{b}_{lm}^\dagger + \hat{b}_{lm}).$$

Substituting this to (A.1) gives the quantum operator for the electric field of the quasistatic mode which is needed to obtain the nanoparticle–QE couplings.

For the dipole modes, it is often more convenient to use the corresponding components of electric dipole moment μ_d (where d labels one of the Cartesian axes x, y and z) instead of η_{1m}. In that case we find

$$\hat{\mu}_d = \sqrt{2\pi\varepsilon_0 R^3 \omega_1 \hbar} (\hat{b}_d^\dagger + \hat{b}_d).$$

Acknowledgments

This work was supported by the Academy of Finland through its Centres of Excellence Programme (2012–2017) and under project Nos. 284621, 303351 and 307419, and by the European Research Council (ERC-2013-AdG-340748-CODE).

References

1. S. Balci and C. Kocabas, *Opt. Lett.* **40**, 3424 (2015).
2. R. Chikkaraddy *et al.*, *Nature* **535**, 127 (2016).
3. C. Cohen-Tannoudji, J. Dupont-Roc and G. Grynberg, *Processus d'Interaction entre Photons et Atomes* (EDP Sciences, Les Ulis, 2000).
4. A. Delga *et al.*, *Phys. Rev. Lett.* **112**, 253601 (2014).
5. A. Delga *et al.*, *J. Opt.* **16**, 114018 (2014).

6. R. H. Dicke, *Phys. Rev.* **93**, 99 (1954).
7. D. Fredkin and I. Mayergoyz, *Phys. Rev. Lett.* **91**, 253902 (2003).
8. M. Gaudin, *J. Phys. (France)* **37**, 1087 (1976).
9. A. González-Tudela *et al.*, *Phys. Rev. Lett.* **110**, 126801 (2013).
10. T. Gruner and D.-G. Welsch, *Phys. Rev. A* **53**, 1818 (1996).
11. J. J. Hopfield, *Phys. Rev.* **112**, 1555 (1958).
12. P. M. Morse and H. Feshbach, Solutions of Laplace's and Poisson's equations, in *Methods of Theoretical Physics, Part II* (McGraw-Hill, New York, 1953), pp. 1264–1265.
13. F. Pan *et al.*, *Phys. Lett. A* **341**, 94 (2005).
14. A. Penzkofer and J. Wiedmann, *Opt. Commun.* **35**, 81 (1980).
15. R. Ruppin, *J. Chem. Phys.* **76**, 1681 (1982).
16. A. Salomon *et al.*, *Phys. Rev. Lett.* **109**, 073002 (2012).
17. E. Sanchez-Burillo *et al.*, *Phys. Rev. Lett.* **113**, 263604 (2014).
18. K. Santhosh *et al.*, *Nat. Commun.* **7**, 11823 (2016).
19. M. Sukharev and A. Nitzan, *Phys. Rev. A* **84**, 043802 (2011).
20. C.-T. Tai, in *Dyadic Green Functions in Electromagnetic Theory* (IEEE Press, Piscataway, N.J., 1994), pp. 210–218.
21. T. Sverre Theuerholz *et al.*, *Phys. Rev. B* **87**, 245313 (2013).
22. P. Törmä and W. L. Barnes, *Rep. Prog. Phys.* **78**, 013901 (2015).
23. M. Wubs, L. G. Suttorp and A. Lagendijk, *Phys. Rev. A* **70**, 053823 (2004).
24. G. Zengin *et al.*, *Phys. Rev. Lett.* **114**, 157401 (2015).
25. Santa Cruz Biotechnology, Rhodamine 6G: Product database (2016), http://www.scbt.com/scbt/misc/datasheeet.jsp.
26. Science Lab.com, Rhodamine 6G: MSDS (2016), http://www.sciencelab.com/msds.php?msdsld=9927579.